Mathematical Biosciences and Engineering

MBE, 18(4): 4508–4527.
DOI: 10.3934/mbe.2021229
Received: 25 March 2021
Accepted: 06 May 2021
Published: 25 May 2021

http://www.aimspress.com/journal/MBE

Research article

The research on minimizing the induction between the transmitting and receiving coils in close range transient electromagnetic inspection of groundwater-related defects in the operating tunnels

Zongyang Li, Taiyue Qi*, Shaojie Qin and Wangping Qian

School of Civil Engineering, Southwest Jiaotong University, Chengdu, Sichuan 610031, China

***Correspondence:** Email: qitaiyue58@126.com.

Abstract: The striking dominance of groundwater-related defects in the operational high-speed railway tunnels in China calls for swift and accurate detection and identification. Thus, it is a new attempt to detect the water-bearing defects at 5 to 10 meters via train-borne transient electromagnetic method in operating tunnels. Due to the short detection distance, the interaction between transmitting and receiving coils is more important than those normally used coils. Thus, numerical and experimental methods are combined to investigate the mutual induction. The influence of turns, current and coil size on the mutual induction and the impact of damping coefficient on the receiving system are manifested. To further verify these findings, full-scale model experiments are conducted. During these physical experiments, the detection results of different coil parameters including coil size, number of turns, and emission current are compared and analyzed. Then, a special effort to minimize the induction between transmitting and receiving coils is expended to acquire the suitable coils for close range detection in the tunnel context. Finally, in order to verify the availability of the detection system, different detection distances are conducted. It turns out that different detection distances have slight difference at the detection results, but they are still within the measuring range of the detection instrument. Obviously, these findings can provide theoretical support for the detection of water-bearing anomalies in operating tunnels and it also has reference significance for the detection of anomalies at close distance.

Keywords: Transient electromagnetic method (TEM); close-range detection; coil induction; tunnel defects; water-bearing anomaly

1. Introduction

The pressing fact that the inefficiency of traditional manual detection method for defects in operational tunnels over the explosive growth of high-speed railway tunnels in China in recent years, plus the detection and maintenance time window for tunnels in high-speed railway lines is strictly limited, propels an innovative approach to ease the plight [1,2]. Here, the defects in operational tunnels refer to the water-bearing anomalies located at 5 to 10 meters from the detection system outside the tunnel lining caused by water accumulation, particularly in the rainy season [3,4]. Figure 1 shows the groundwater hazard caused by the water-bearing anomaly behind the tunnel lining in the high-speed railway tunnel. Thereby a novel train-borne transient electromagnetic method (TEM) designated for water-bearing defects in operational tunnels comes into emergence, shown as Figure 2. The prominent characteristic is the close detection distance, as most of the TEM detection distance performed in tunnels are tens of meters or more [5,6].

Figure 1. The example of groundwater disaster in operational high-speed railway tunnel.

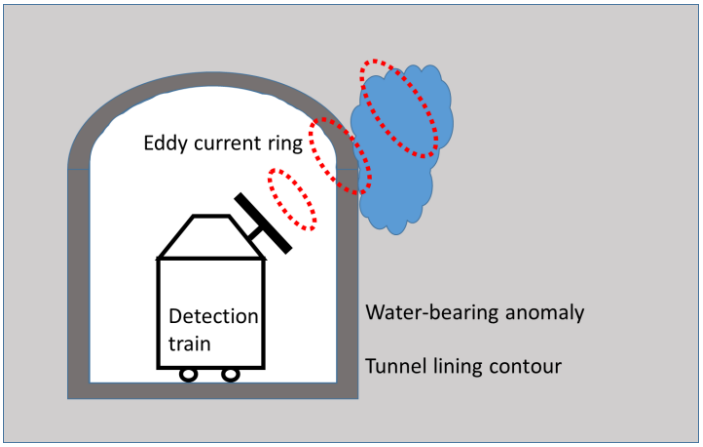

Figure 2. Detection diagram of the automatic detection train.

It is obvious that in any TEM detection, the induction process between the transmitting and receiving coils is always existed. But most TEM detections omit the induction process due to it only affects the early data [7,8]. The example of Protem-47, which is used for the medium and long range detection, could explain the situation, shown as the Figure 3. The original provided coil has a length of 70 meters with 8 turns inside. The corresponding turn-off time it introduces is over 5 microseconds let alone the turn-off time caused by the TEM processor. To most general cases, the early induction process doesn't affect the detection for the medium and long range targets. But for this close range TEM detection in tunnels, certainly it cannot meet the requirements. To be elaborated, Figure 4 shows the numerical results of the same anomaly at different distances (10 and 20 meters), which clearly shows the importance of the early data at around 1e-6 s for anomalies at a distance of 10 m, while it does not affect anomalies at a distance of 20 m (marked by a red line in Figure 4). And the closer the target is, the more important the early data are [9,10]. If the induction process between coils were not properly suppressed, early detection data would fail to reflect the anomaly at this close range [11]. Therefore, the induction process must be fully investigated in order to redesign the suitable coils for the application.

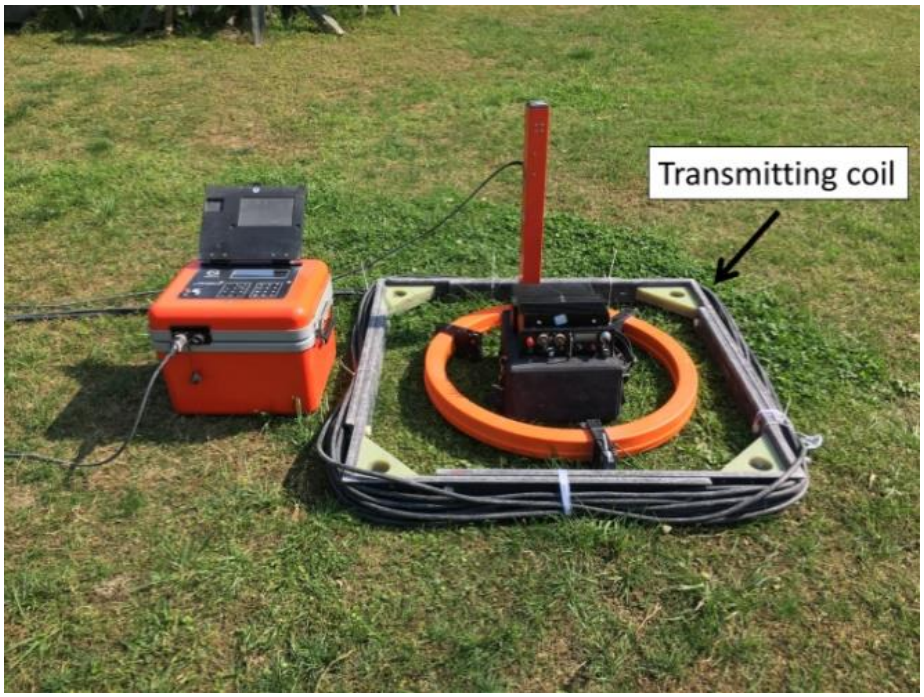

Figure 3. Protem-47 and the original coils provided by manufacturer.

Moreover, multi-turn small loops, rather than the commonly-used large size TEM loops, are often applied to forecast the water-bearing anomalies in tunnels due to the confined space. However, adding turns in coils causes serious impact on the distortion time, which will prolong the turn-off time in the transmitting system. Thus, Fitterman and Anderson (1987) presented a general procedure for computing the effect of non-zero turn-off time on the transient electromagnetic response on the foundation of central loop configuration [12]. Kamenetsky and Oelsner (2008) first started to estimate minimum time-delay after which these distortions may be neglected using the equivalent lumped circuit diagram of the transmitting loop [13]. Besides, different correction methods have also been put

forward. Such as Sun (2008) studied the effect of transmitting waveform under different geological conditions on TEM detection results and the method of correction [14]. Bai and Meju (2001) discussed the effect of two types of turn-off current on the TEM response and the correction techniques [15]. Thereby, it is of great significance to optimize the detection system to have a minimal distortion for this close-range detection (5–10 m) of train-borne TEM [16].

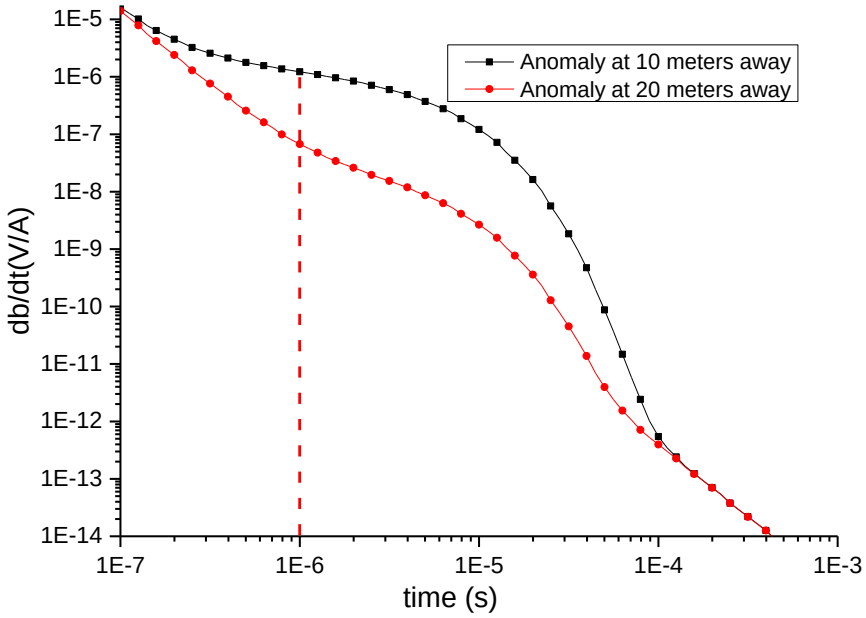

Figure 4. The diagram of detection results of anomalies at different close distances.

In order to analyze the influencing factors, the mechanism of the TEM detection system will be first discussed. Then the impact of factors concerning detection coils on the mutual induction process will be elaborated with the aid of numerical simulation. Further the influence of damping coefficient on the receiving system is also analyzed by calculation. At last, the coils suitable for the tunnel context are putting forward by the full-scale close-range TEM model. In this process, the situations of different detection distances are also tested to verify the practicality of the designed coils.

2. Mechanism of the TEM detection system

In the TEM detection process, the transmitting loop serves as a vehicle for giving out a certain magnetic moment, which is related to the current, coil size and coil turns. Due to the propagation of this magnetic moment, both the detection objective (normally tagged as anomaly) and the medium render electromagnetic induction according to their own resistivity. Then, the receiving loop records the entire electromagnetic induction process from the target and the medium [17].

Therefore, it can be concluded that the detection results in the receiving loop reflect the electromagnetic properties of the anomalies and the medium. During the process, the emitted magnetic moment acts only as a trigger to induce electromagnetic induction in the anomalies and the medium, which are not related to the shape of the response curve, but affect the amplitude of the curve. Figure 5 and Figure 6 have demonstrated that changing the current and the coil radius of the transmitting loop, other things being the same, does not affect the shape of the detection curve (both of which are factors that affect the magnetic moment).

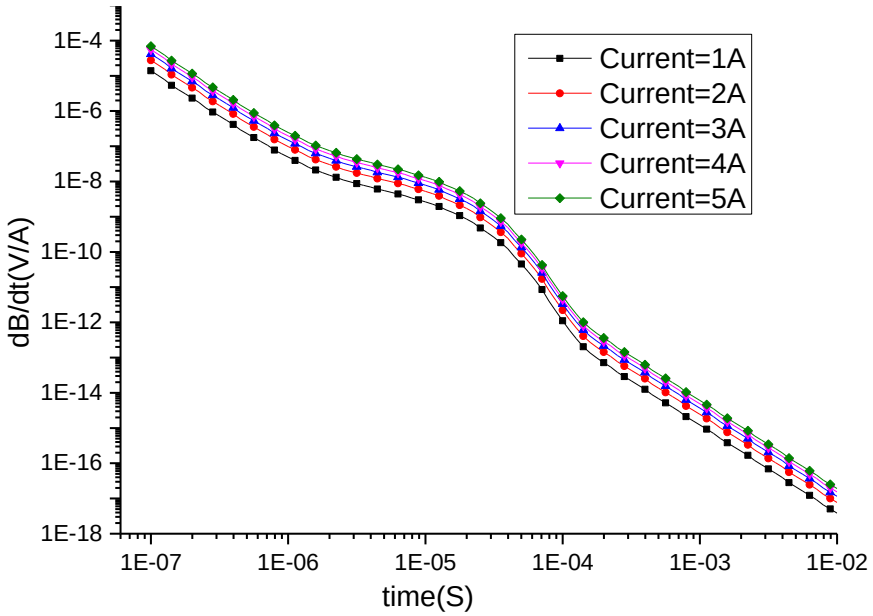

Figure 5. Detection results of different current when other conditions remain the same.

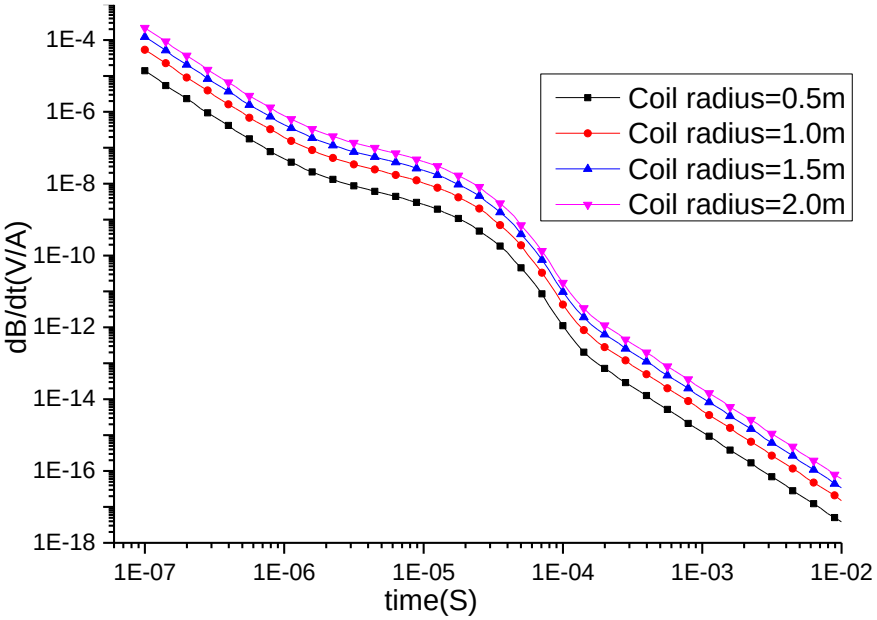

Figure 6. Detection results of different coil radius when other conditions remain the same.

However, in practice the presence of transmitting and receiving loops would introduce a mutual induction process, also known as the transient process, which would bias the detection results at an early stage. For this reason, under normal circumstances, the design of the detection system follows the principle that the transmitting magnetic moment should be large enough to ensure that the response curve falls into the detection range that can be recorded by the existing TEM processor, meanwhile the transmitting and receiving loops should cooperate to minimize the transient process in order to obtain an accurate early response.

From above depiction, an interesting situation emerges, namely the fact that the emitted magnetic moment needs to be as large as possible to obtain a clear detection result after satisfying the minimum

accuracy of the detection instrument collides with the demand to diminish the magnetic moment to suppress the turn-off effect or the mutual induction process between the transmitting loop and receiving loop.

At some specific occasions where the space is constrained, the loop size is limited, as in the tunnel context. In order to raise the resolution, often the means of increasing the current and coil turns is utilized. This normal procedure, in most cases, is applicable for anomalies with no prior distance information. However, what the train-borne TEM aims to in this paper is the water-bearing anomalies located outside the tunnel lining (5–10 m). Therefore, it is of great importance to investigate the influence of each parameter on the induction process before proceeding with the design of the detection coils for this close-range TEM detection.

3. Impact of the coil parameters on mutual induction process

As mentioned earlier, the mutual induction process between the transmitting and receiving coils is the cause of the early data distortion, while the mutual induction is caused by the sudden change of the turn-off current. Thus, in this segment, in order to have a clear insight into the mutual induction process, the three coil factors concerning the magnetic moment in the transmitting coil will be simulated for their impact on the mutual induction process. First, a 10-turn transmitting coil with 1 m radius and a 10-turn receiving coil with 0.5 m radius are set as basic configuration, on which variant parameters are developed. The excitation in the transmitting coil to initiate the mutual induction process is an ideal step turn-off current 1 A. Then the receding process of the induced voltage in receiving coils is recorded. By changing the parameters of the transmitting coil, it readily unveils the influence of different parameters on the mutual induction process. The effects of different radii, number of turns and initial currents on the mutual inductance process are given respectively in Figure 7, Figure 8 and Figure 9. It should be noted that among these three factors only the current factor does not change the shape of the curve, but makes it fluctuate at different magnitudes.

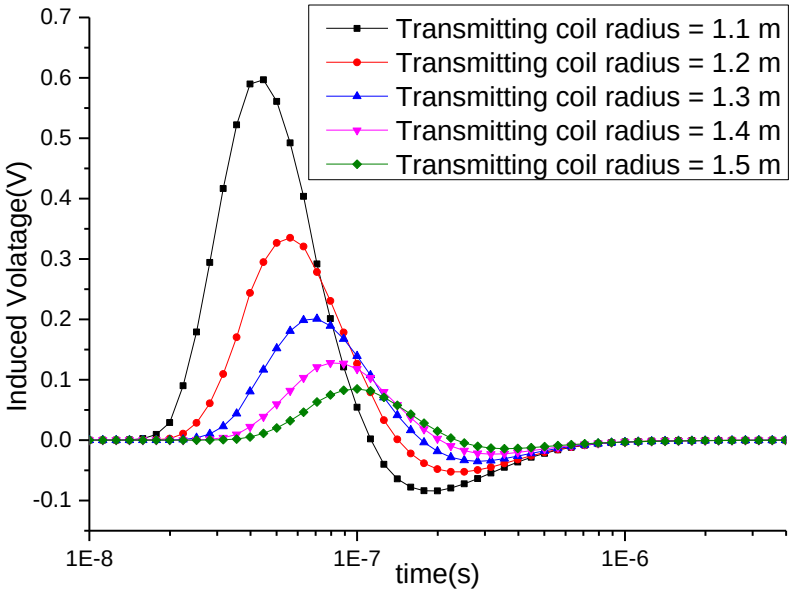

Figure 7. Induced voltage in the receiving coils caused by variant radii of transmitting coils.

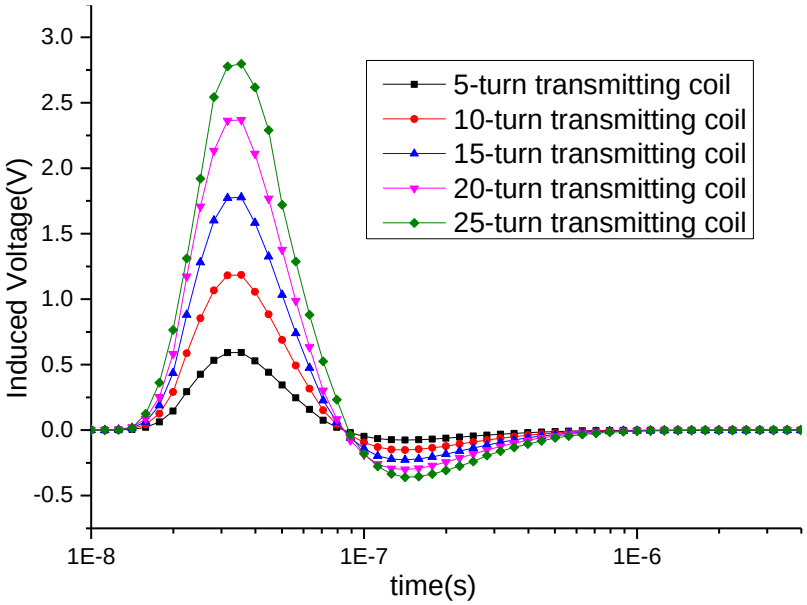

Figure 8. Induced voltage in the receiving coils caused by variant turns of transmitting coils.

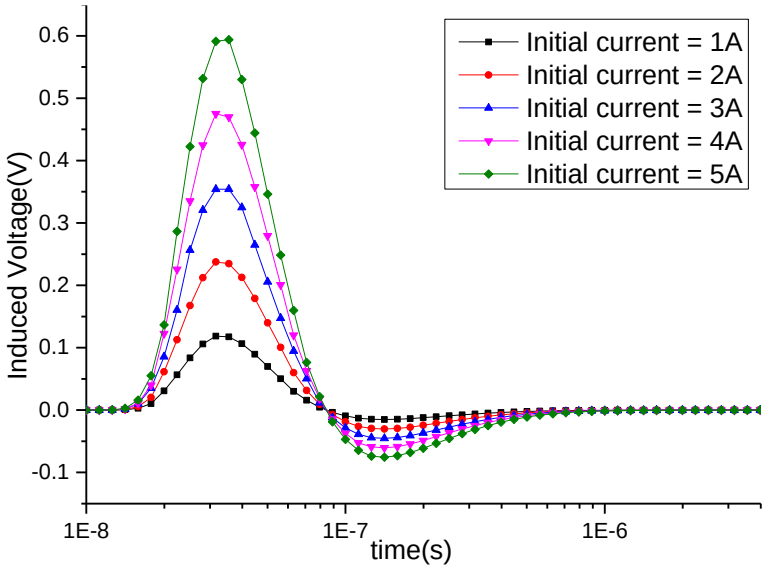

Figure 9. Induced voltage in the receiving coils caused by variant initial currents of transmitting coils.

In the same manner, the parameters of receiving coils can be simulated. Figure 10 and Figure 11 show the profound effects of different receiving coil radii and number of turns on the mutual inductance process, respectively.

The above results verify that the size and turns of both the transmitting and receiving coils have an effect on the mutual induction, while the magnitude of the transmitting current determines the magnitude of the mutual induction; the larger the current, the greater the induction magnitude, and vice versa.

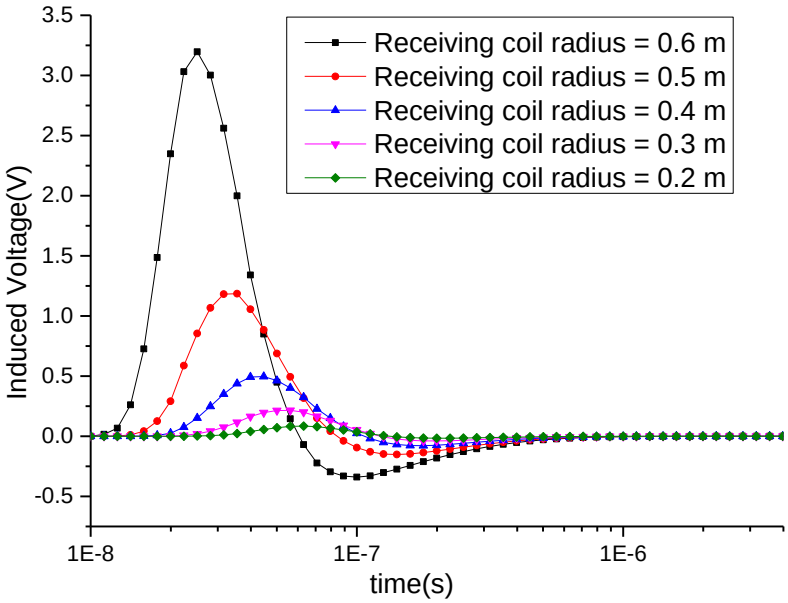

Figure 10. Induced voltage in the receiving coils caused by variant radii of receiving coils.

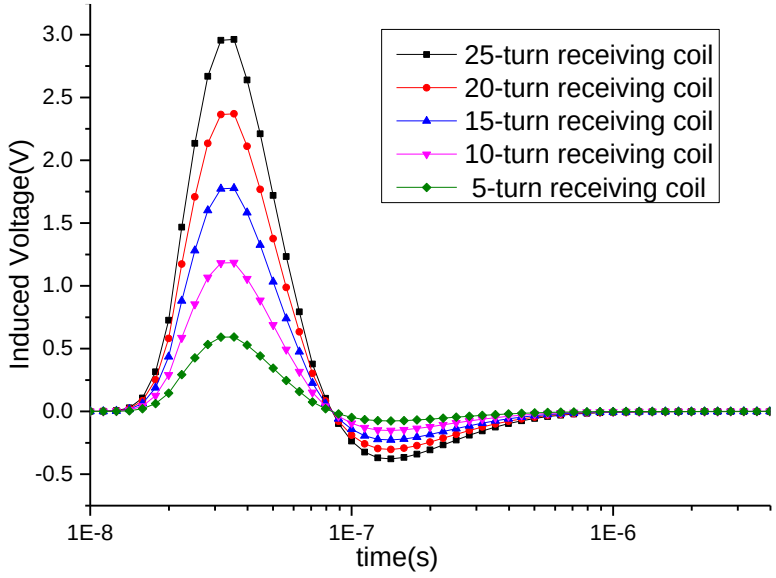

Figure 11. Induced voltage in the receiving coils caused by variant turns of receiving coils.

4. Impact of the parameters of the receiving coil on mutual induction process

To facilitate the study, the equivalent circuit diagram of the TEM receiving loop could be sketched as Figure 12, where E is the induced voltages received in the loops; r, L and C represent the resistance, inductance and capacitance of the receiving loop respectively; R denotes the damping resistance paralleled in the receiving loop and V signifies the voltages observed through preamplifier [18].

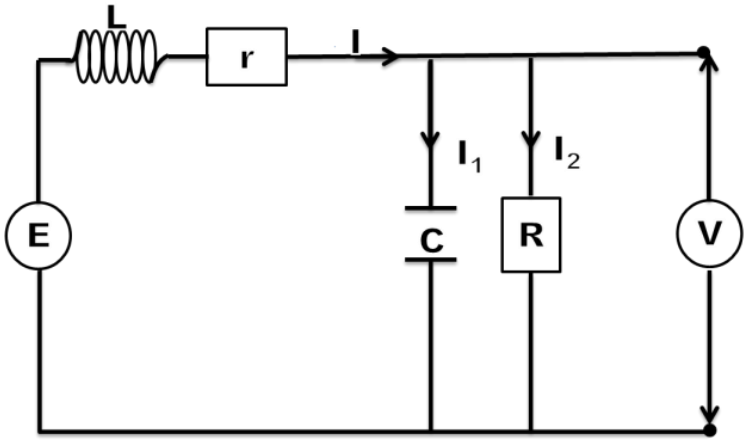

Figure 12. Sketch of the equivalent circuit diagram of the TEM receiving loop.

The circuit equation corresponding to the Figure 12 could be written as:

$$E = L\frac{dI}{dt} + Ir + V \tag{1}$$

$$I = C\frac{dV}{dt} + \frac{V}{R} \tag{2}$$

Formula (1) and (2) could combine as:

$$E = LC\frac{d^2V}{dt^2} + (rC + \frac{L}{R})\frac{dV}{dt} + (\frac{r}{R} + 1)V \tag{3}$$

Formula (3) is rewritten as:

$$\frac{E}{LC} = \frac{d^2V}{dt^2} + 2\delta\frac{dV}{dt} + \omega_p^2 V \tag{4}$$

In equation (4):

$$\delta = \frac{1}{2}\left(\frac{r}{L} + \frac{1}{RC}\right) \tag{5}$$

$$\omega_p = \sqrt{\frac{1}{LC}\left(\frac{r}{R} + 1\right)} = \omega_0\sqrt{\frac{r}{R} + 1} \tag{6}$$

Where ω_p and ω_0 signify respectively the resonant frequency and natural resonance frequency of the coil. The damping coefficient could be defined as:

$$\zeta = \frac{\delta}{\omega_p} = \frac{RrC+L}{2\sqrt{LCR(r+R)}} \tag{7}$$

And:

$$\beta = \sqrt{|\delta^2 - \omega_p^2|} \tag{8}$$

$$\delta = \zeta\omega_p \tag{9}$$

Then the formula (4) could be replaced as:

$$\frac{d^2V}{dt^2} + 2\zeta\omega_p\frac{dV}{dt} + \omega_p^2 V = \frac{E}{LC} \tag{10}$$

The initial condition for (10) can be expressed as:

$$\begin{cases} V|t = 0 = \eta \\ \frac{dV}{dt}|t = 0 = \varepsilon \end{cases} \tag{11}$$

where η and ξ are constants.

4.1. The relation between damping resistance and damping coefficient

The characteristic equation for second order linear differential equation with constant coefficients could be expressed as:

$$\lambda^2 + 2\zeta\omega_p\lambda + \omega_p^2 = 0 \tag{12}$$

The discriminant for equation (12) can be rewritten as:

$$\Delta = \left(2\zeta\omega_p\right)^2 - 4\omega_p^2 = 4\omega_p^2(\zeta^2 - 1) \tag{13}$$

Due to$\zeta \geq 0$:

$$\zeta = 1 \tag{14}$$

At this point, the circuit is in critical damping state. When $\zeta > 1$ the circuit is in over damping state or when $\zeta < 1$ the circuit is in under damping state. Equation (7) can be varied as:

$$R = \frac{(1-2\zeta^2)r \pm 2\zeta\sqrt{(\zeta^2-1)r^2 + \frac{L}{C}}}{4\zeta^2 - r^2\frac{C}{L}} \tag{15}$$

When critical damping state takes place, damping resistance R can be calculated as:

$$R = \frac{L}{rC + 2\sqrt{LC}} \tag{16}$$

Another root is omitted for below 0. Thus, the relation between damping resistance and damping coefficient can be portrayed as Figure 13.

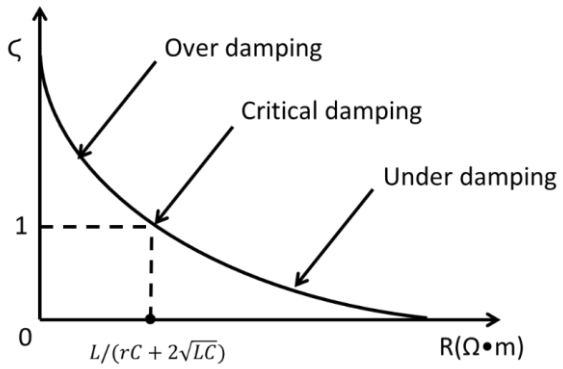

Figure 13. Sketch of the relation between damping resistance and damping coefficient.

4.2. The features of the receiving loops concerning damping coefficient

System transfer function could be obtained by Laplace transformation of Equation (10) as:

$$h(s) = \frac{v(s)}{\varepsilon(s)} = \frac{1}{LC\left(s^2+2\zeta\omega_p s+\omega_p^2\right)} \tag{17}$$

The amplitude frequency characteristic of the receiving system can easily be expressed with system transfer function (17) as:

$$H(f) = \frac{1}{LC\sqrt{\omega_p^4+8\pi^2 f^2\left[2\pi^2 f^2+\omega_p^2(2\zeta^2-1)\right]}} \tag{18}$$

Function (18) is sketched as Figure 14.

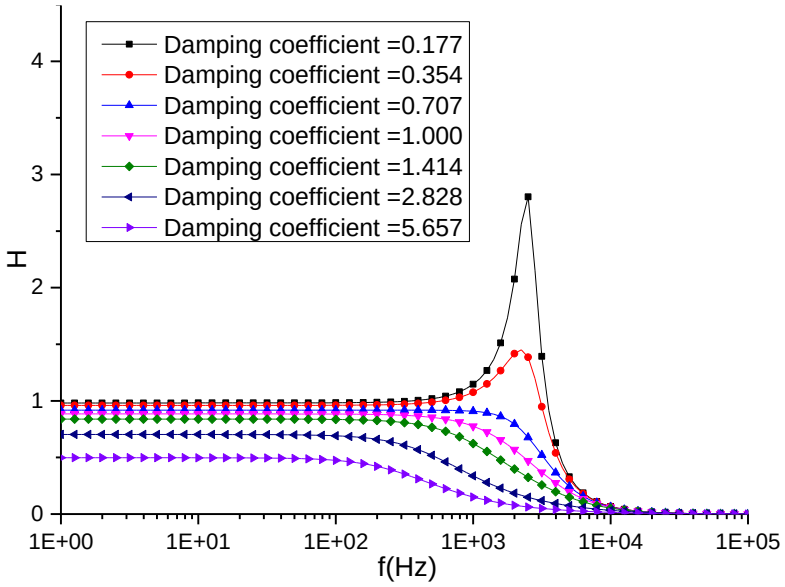

Figure 14. Sketch of variation of the amplitude frequency characteristic of the receiving system on damping coefficient.

It is evident that signal gain decreases along with the increase of damping coefficient. Moreover, there is a resonant frequency in the system when $\zeta \leq \sqrt{2}/2$.

Another feature worth noting is the cut-off frequency in the system when damping coefficient varies, which is defined as $1/\sqrt{2}$ of the maximum amplitude:

$$f_b = \frac{\omega_p}{2\pi}\sqrt{1 - 2\zeta^2 + \sqrt{4\zeta^4 - 4\zeta^2 + 2}} \tag{19}$$

The relation between the cut-off frequency and damping coefficient is mapped as Figure 15.

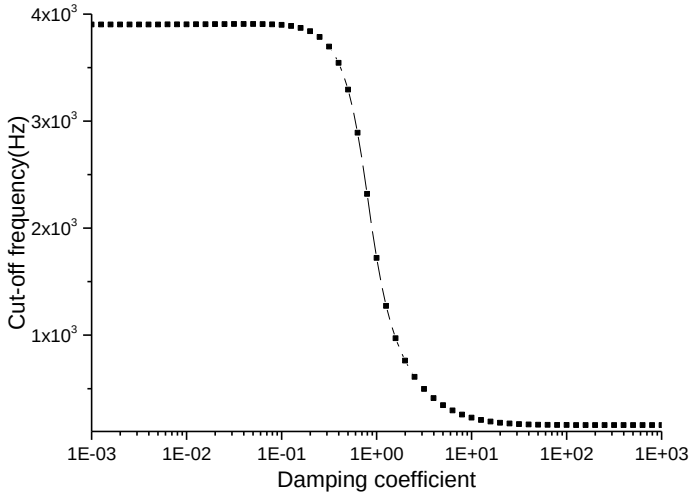

Figure 15. Sketch of relation between the cut-off frequency and damping coefficient.

The impulse response of the receiving system could be calculated by inverse Laplace transformation of system transfer function (17) as:

$$h(t) = L^{-1}[h(s)] = \begin{cases} \frac{1}{LC\beta} e^{-\delta t} sh(\beta t), \zeta \geq 1 \\ \frac{1}{LC\beta} e^{-\delta t} \sin(\beta t), \zeta < 1 \end{cases} \tag{20}$$

The relation between the impulse response of the receiving system and damping coefficient is mapped as Figure 16.

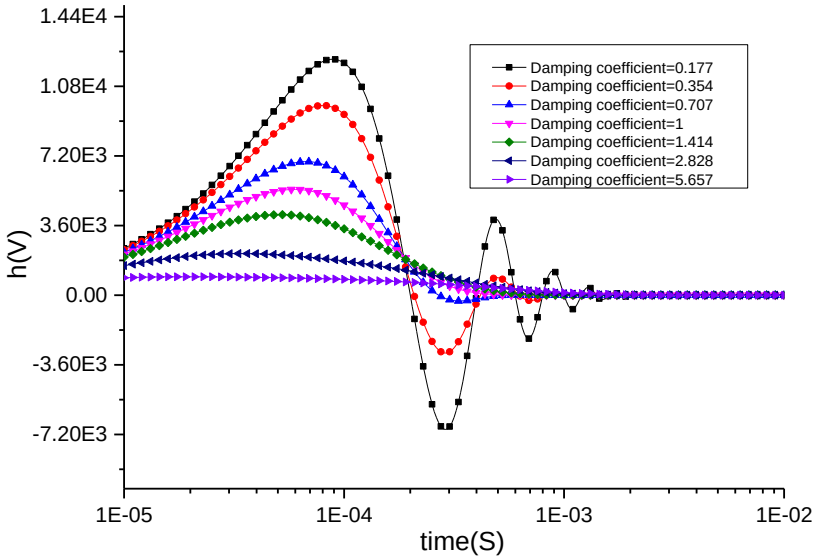

Figure 16. Sketch of relation between the impulse response of the receiving system and damping coefficient.

The step response of the receiving system could be calculated by inverse Laplace transformation of quotient of system transfer function (17) divided by S as:

$$u(t) = L^{-1}\left[\frac{1}{s}h(s)\right] = \begin{cases} \frac{1}{LC\omega_p^2}\left\{1 - e^{-\delta t}\left[ch(\beta t) + \frac{\delta}{\beta}sh(\beta t)\right]\right\}, \zeta \geq 1 \\ \frac{1}{LC\omega_p^2}\left\{1 - e^{-\delta t}\left[cos(\beta t) + \frac{\delta}{\beta}sin(\beta t)\right]\right\}, \zeta < 1 \end{cases} \tag{21}$$

The relation between the step response of the receiving system and damping coefficient is mapped as Figure 17.

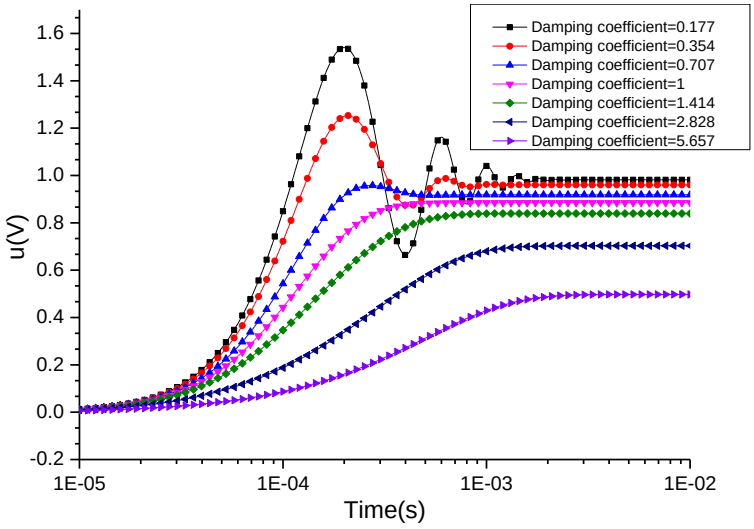

Figure 17. Sketch of relation between the step response of the receiving system and damping coefficient.

4.3. Comprehensive analysis of the impact of damping coefficient on the receiving system

From above depiction, it is clear that the damping coefficient determines the receiving system's response to the excitation. To be elaborated, the increase of damping coefficient renders the rising time of the response curves prolonged, delays the response speed to the excitation, reduces the cut-off frequency and amplitude, and also highlights the low frequency characteristic of the receiving system. In summary, the critical damping state ($\zeta = 1$) is optimum, which exhibits that the curves of impulse response and step response avoid oscillation phenomenon with moderate amplitude and acceptable signal attenuation. Consequently, a favorable receiving system ought to have high cut-off frequency to broaden the effective probing range and to be close to the critical damping state to avoid the oscillation phenomenon as much as possible.

5. Verification of the effect of different damping coefficients on detection results

According to the previous analysis, it is certain that the induced voltage caused by the low resistance body and the induced voltage displayed by the instrument are not equal in value. From the signal point of view, their relationship can be defined as the input and output of a signal system. However, people usually mix them as one thing. To illustrate the influence of damping coefficient, an ideal detection curve of rock background with the resistivity 10^4 Ω•m is taken as the input of a receiving system, while the parameters of the receiving coil is: r = 2 Ω, L = $2 \cdot 10^{-3}$ H, C= $2 \cdot 10^{-6}$ F. Therefore, based on the knowledge of linear time-invariant theory, the output of the receiving system with different damping coefficients can be sketched as Figure 18, where the discrepancy between different damping coefficients is staggering.

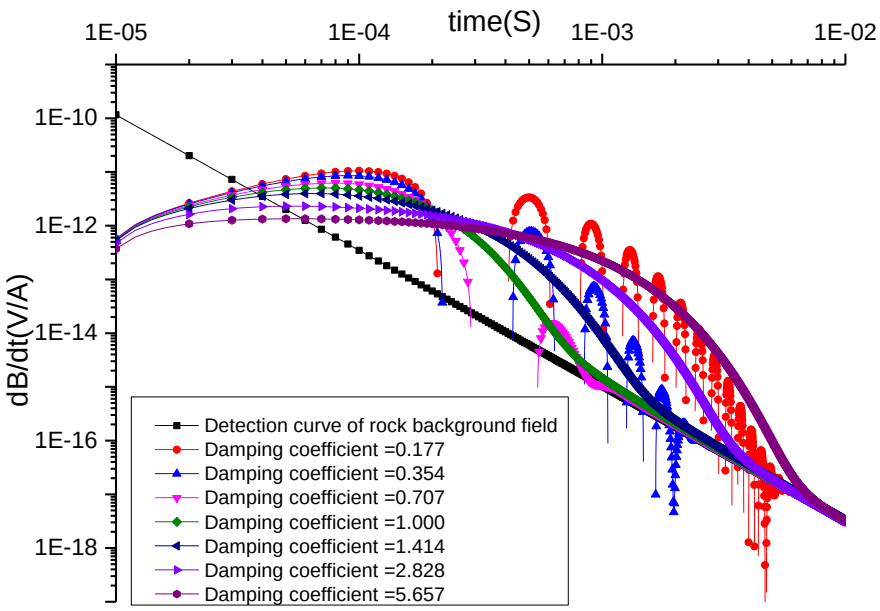

Figure 18. The impact of different damping coefficient of the receiving system on the detection curve.

From Figure 18, it could be seen that in critical damping state ($\zeta = 1$), the output curve is the earliest one to merge into the input one, i. e. it takes the least amount of distortion time to output the true value of the probe; when the damping factor is gradually greater than 1, it takes more time for the output curve to converge with the input one. Meanwhile, in under damping state ($\zeta < 1$), the output curve is accompanied by an oscillation phenomenon. In general, all the output curves have experienced an upward trend and a gradually decline trend to converge with the input one. This is also reflected by the common TEM detection results, where the data of early times has a distinctive discrepancy to the theoretical result putting aside the mutual induction process and the data of late times renders to be consistent with the theoretical result; i.e., damping coefficient of the receiving system has a great impact on the shallow layer prospecting and little influence on the deep layer prospecting.

6. Redesigning of the transmitting and receiving coils for close-range TEM detection

To ensure the train-borne TEM detection system to work in optimal condition with minimum distortion for the anomaly as shown in the Figure 2, it is bound to redesign the transmitting and receiving coils due to the coils the manufacturer provided are not suitable for the case in tunnels. Moreover, it is evident that the resistance of the coils and the damping resistance are prone to measure. But the inductance and capacitance of the loops cannot be easily measured and validated, let alone the instability of the inductance and capacitance to subtle space change between coils. Therefore, we directly test different combinations of transmitting and receiving loops. Due to space limitation of the high-speed railway tunnels and portability of the coils, both the transmitting and receiving coils are designed as square coils and the side length should within 1.5 m.

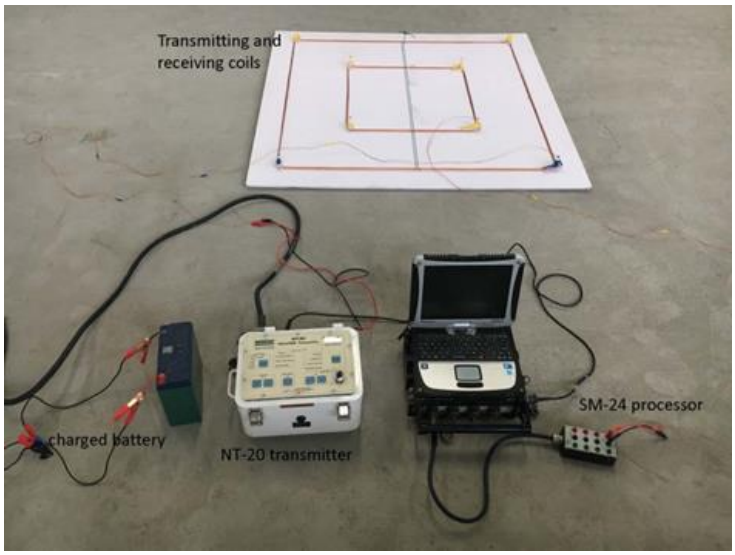

Figure 19. The demonstration of TEM transmitter and processor for detection.

The transmitting loop's side length chooses from 1.5m, 1.2m, 1m, 0.8m, while the receiving loop's side length chooses from 1.2m, 1m, 0.8m and 0.5m. The turns of each coil should not exceed 10. And the current varies from 0.5 A to 2 A. Moreover, the TEM transmitter is NT-20 and TEM

processor is SM-24 shown as Figure 19, both are renowned for close-range detection. The water-bearing anomaly is simulated by the water bag filled up with dilute brine. It is supported by the horizontally laid shield segments shown as Figure 20. The actual case is showed by Figure 2. The detection distance is set at 7 m, which is in the middle of 5 to 10 m.

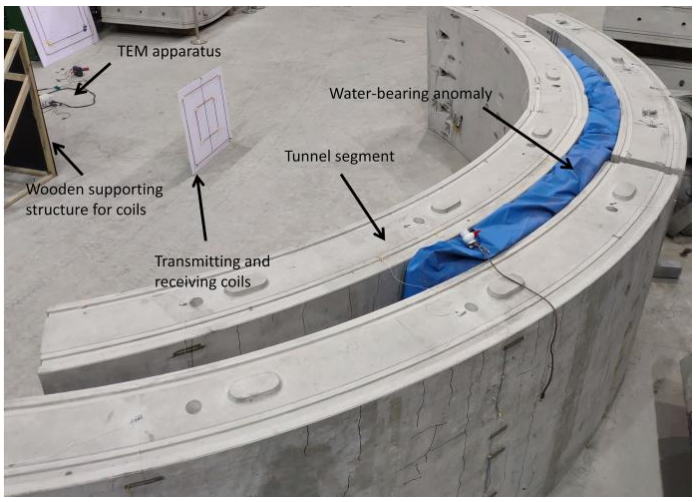

Figure 20. The sketch map of the experiment.

After comparing of different combination, we will display some typical situations to verify the conclusions made by former part. First, the receiving coil remains unchanged; the transmitting coil changes its side length and turns, the results are shown as Figure 21. It is clear that there are oscillations in some of the curves in Figure 21 due to the difference in excitation.

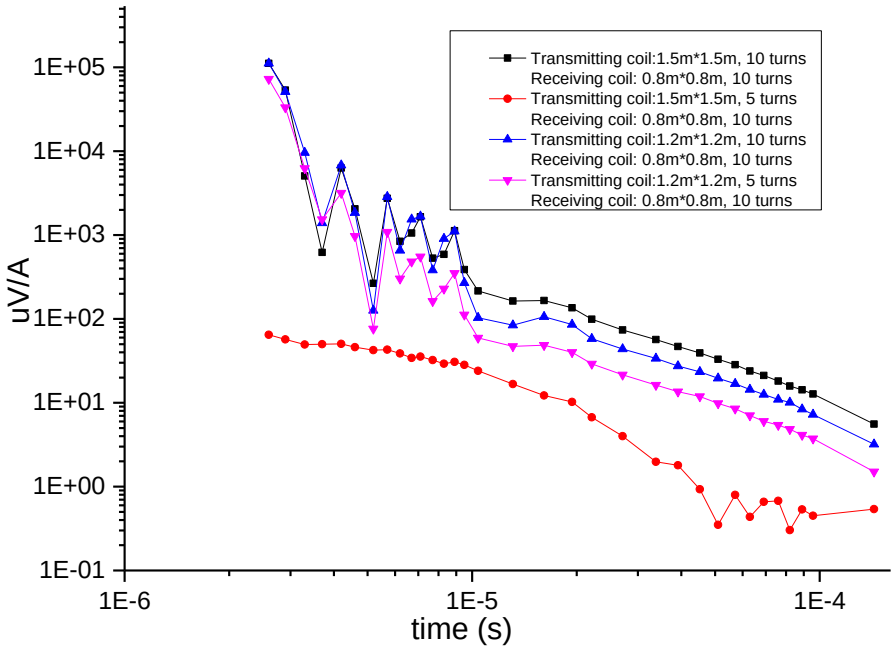

Figure 21. The transmitting coil changes its parameter while the receiving coil remains identical.

Figure 22 clearly demonstrates the response of three different receiving systems to an identical input, which contains three types of detection curves caused by different damping coefficients. The blue curve with oscillation phenomenon could be deemed in under damping state. The black curve with minor response could be regarded as in over damping state. At last, the red curve with satisfying response is presented, which could accurately reflect the anomaly information.

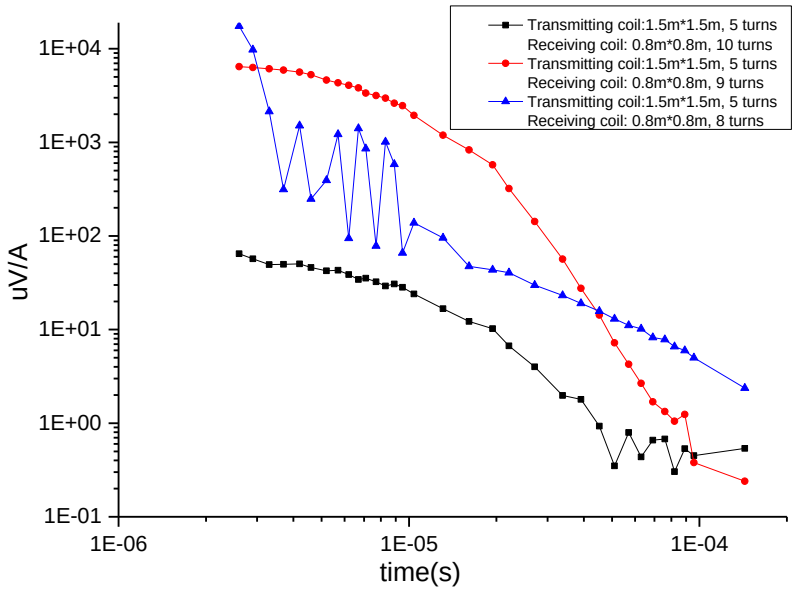

Figure 22. The receiving coil changes its parameter while the transmitting coil remains identical.

Figure 23 shows the current impact on detection results. Different current renders different turn-off time. But three detection curves have only amplitude variance apart from the turn-off time, which is also verified in Figure 5.

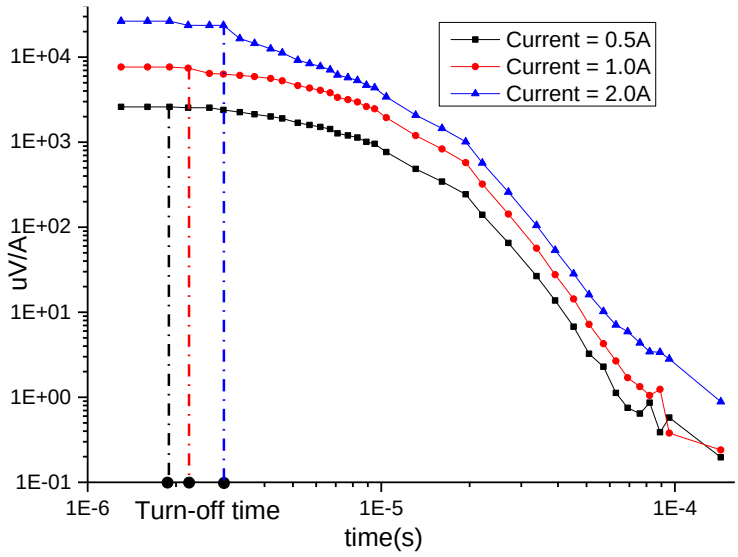

Figure 23. The current's impact on detection results.

Since the water-bearing anomaly locates at different positions from 5 m to 10 m, in order to verify the availability of the detection coils, different detection distances are conducted. The detection results are shown in Figure 24. The different detection distances prove to have a slight effect on the curve amplitude, however, all the curves are within the measurement range of the TEM instrument, which means that the newly designed coil can meet the requirements of different detection distances in the tunnel.

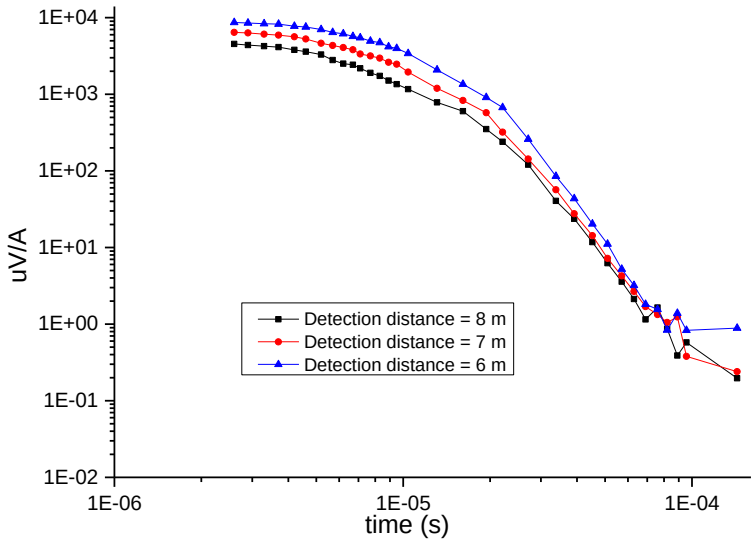

Figure 24. Detection results of different distance.

7. Conclusion

This paper focuses on the technical points related to the mutual induction between the coils according to the requirements of the close range detection after explaining the necessity of redesigning the coil in the close range TEM detection. To be specific, the mechanism of TEM detection is first clarified to facilitate later analysis. Then, due to the requirements of proximity detection, the mutual induction process between the transmitting and receiving coils caused by the turn-off current is discussed with the aid of numerical simulation. The impact of turns, current and coil size, which are related to the magnetic moment, on the mutual induction process is thoroughly studied. The result shows that all these three factors affect the mutual induction process significantly and only the current factor doesn't change the curve shape but influences the amplitude.

Subsequently, the emphasis is placed on the receiving system. The influence of damping coefficient on the receiving system is examined. The conclusion can be summarized that the critical damping state is optimal. In under damping state, the output curve is accompanied by oscillation phenomenon, while in over damping state, it takes more time for the output curve to converge with the theoretical one.

At last, the full-scale close-range TEM detection experiment is conducted. The experiment verified the conclusion of the impact of factors concerning magnetic moment on mutual induction process. And three different conditions of the damping coefficient in the receiving system have also

been presented. Further, the availability of the detection system for various detection distances is tested. The results have proved that the newly designed detection system satisfies the requirements for close-range TEM detection, which lays the foundation for future train-borne TEM usage in tunnel context.

Data Availability

The data used to support the findings of this study are available from the corresponding author upon request.

Acknowledgment

It is of great appreciation for the constructive remarks and suggestions of the reviewers and editors. Also, we'd like to take this opportunity to express gratitude for the support from National Natural Science Foundation of China (grant No. 51278423, grant No. 51478395 and grant No.51978582) and from 2021 Nantong Science and Technology Plan Project (grand No. 75).

Conflicts of interest

The authors declare that there are no conflicts of interest regarding the publication of this paper.

Reference

1. C. X. Liu, Cause Analysis and construction technology study of water-leakage of liner in Huangdengxian Tunnel, *J. Railw. Sci. Eng.*, **2** (2010), 79–82.
2. P. Li, Displacement characteristics of high-speed railway tunnel construction in loess ground by using multi-step excavation method, *Tunn. Undergr. Sp. Tech.*, **51** (2015), 41–55.
3. X. Liang, T. Qi, Z. Jin, W. Qian, Hybrid support vector machine optimization model for inversion of tunnel transient electromagnetic method, *Math. Biosci. Eng.*, **17** (2020), 3998–4017.
4. K. Y. Wang, H.Xiao, Y. J. Shang, K. M. Sun, W. T. He, Prediction of rock burst at wall rocks of tunnels in Southwest, *J. Eng. Geol.*, **5** (2014), 903–914.
5. G. Q. Xue, C. Y. Bai, S. Yan, S. Greenhalgh, M. F. Li, N. N. Zhou, Deep sounding tem investigation method based on a modified fixed central-loop system, *J. Appl. Geophys.*, **76** (2012), 23–32.
6. G.Q. Xue, L. Zhang, N. Zhou, W. Chen, Developments measurements of TEM sounding in china, *Geol. J.*, **55** (2020), 1636–1643.
7. E. Auken, Approaching 10 microsec (and earlier) with the Skytem system, *ASEG Extended Abstracts*, **1** (2010), 1.
8. B. R. Spies, The dual loop configuration of the transient electromagnetic method, *Geophysics*, **40** (1974), 1051.
9. G. Q. Xue, J. L. Cheng, N. N. Zhou, W. Y. Chen, H. Li, Detection and monitoring of water-filled voids using transient electromagnetic method: A case study in shanxi, china, *Environ. Earth Sci.*, **70** (2013), 2263–2270.
10. A. E. Plotnikov, Evaluation of limitations of the transient electromagnetic method in shallow-depth studies: Numerical experiment, *Russ. Geol. Geophys.*, **55** (2014), 907–914.

11. Z. Xi, X. Long, L. Huang, S. Zhou, G. Song, H. Hou, et al., Opposing-coils transient electromagnetic method focused near-surface resolution, *Geophysics*, **81** (2016), E279–E285.
12. D. V. Fitterman, W. L. Anderson, Effect of transmitter turn-off time on transient soundings, *Geoexploration*, **24** (1987), 131–146.
13. F. Kamenetsky, C. Oelsner, Distortions of EM transients in coincident loops at short time-delays, *Geophys. Prospect.*, **48** (2008), 983–993.
14. I. M. Lee, Q. H. Truong, D. H. Kim, J. S. Lee, Discontinuity detection ahead of a tunnel face utilizing ultrasonic reflection: Laboratory scale application, *Tunn. Undergr. Sp. Tech.*, **24** (2009), 155–163.
15. Denghai Bai, Maxwell Meju, The effect of two types of turn-off current on TEM responses and the correction techniques, *Seismology and Geology*, **23** (2001), 245–251.
16. B. R. Spies, D. E. Eggers, The use and misuse of apparent resistivity in electromagnetic methods, *Geophysics*, **51** (1986), 1462.
17. K. Vozoff, Electromagnetic methods in applied geophysics, *Geophys. Surveys*, **4** (1980), 9–29.
18. H. J. Wang, Characteristics of damping coefficient effect on transient electromagnetic signal, *Chin. J. Geophys.*, **53** (2010), 428–434. (*In Chinese*).

AIMS Press